

Tunable Exciton Polaritons in Band-Gap Engineered Hexagonal Boron Nitride

Pedro Ninhos,[†] Christos Tserkezis,[†] N. Asger Mortensen,^{†,‡} and

Nuno M. R. Peres^{*,†,¶,§}

[†]*POLIMA—Center for Polariton-driven Light–Matter Interactions, University of Southern Denmark, Campusvej 55, DK-5230 Odense M, Denmark*

[‡]*D-IAS—Danish Institute for Advanced Study, University of Southern Denmark, Campusvej 55, DK-5230 Odense M, Denmark*

[¶]*Centro de Física (CF-UM-UP) and Departamento de Física, Universidade do Minho, P-4710-057 Braga, Portugal*

[§]*International Iberian Nanotechnology Laboratory (INL), Av Mestre José Veiga, 4715-330 Braga, Portugal*

E-mail: peres@fisica.uminho.pt

Abstract

We show that hexagonal boron nitride (hBN), a two-dimensional insulator, when subjected to an external superlattice potential forms a paradigm for electrostatically tunable excitons in the near- and mid-ultraviolet (UV). With a combination of analytical and numerical methods, we see that the imposed potential has three consequences: (i) it renormalizes the effective mass tensor, leading to anisotropic effective masses; (ii) it renormalizes the band gap, eventually reducing it; (iii) it reduces the exciton binding energies. All these consequences depend on a single dimensionless parameter, which includes the product of strength of the external potential with its period. In addition to

the excitonic energy levels, we compute the optical conductivity along two orthogonal directions, and from it the absorption spectrum. The results for the latter show that our system is able to mimic a grid polarizer. These characteristics make one-dimensional hBN superlattices a viable and meaningful platform for fine-tuned polaritonics in the UV to visible spectral range.

Keywords

hexagonal boron nitride, super lattice, sub-gap optical response, exciton polaritons, photonics

1

The properties of two-dimensional (2D) materials are characterized by a richness of physical phenomena, encompassing unusual elastic,¹ electronic,² and optical properties.³ An exemplary case of enhanced light–matter interactions in 2D materials is provided by graphene,⁴ whose transmission in the visible range of the spectrum is characterized by the value of the fine structure constant alone, a peculiar case in materials. Concerning the electronic properties in 2D materials, we can find semi-metals,⁵ conductors,⁶ semiconductors and insulators,^{7,8} strange metals,⁹ metallic ferromagnets,^{10,11} and superconductors.^{12–15} Therefore, 2D materials have become a condensed-matter physicist’s playground due to this wealth of physical properties. Some systems, such as hexagonal boron nitride (hBN), have an interesting story: the first application of hBN was as an encapsulating medium for graphene and other 2D materials, due to its ultra-flat surface and low density of defects.¹⁶ Such use allows to increase the mobility of charge carriers¹⁷ and produce well defined (large quality factor Q) electromagnetic (EM) resonances in polaritonic devices. Later, it became clear that hBN is interesting in its own right when light–matter interaction is considered.^{18,19} The interaction with infrared radiation due to polar phonons in hBN gives rise to large- Q polaritonic res-

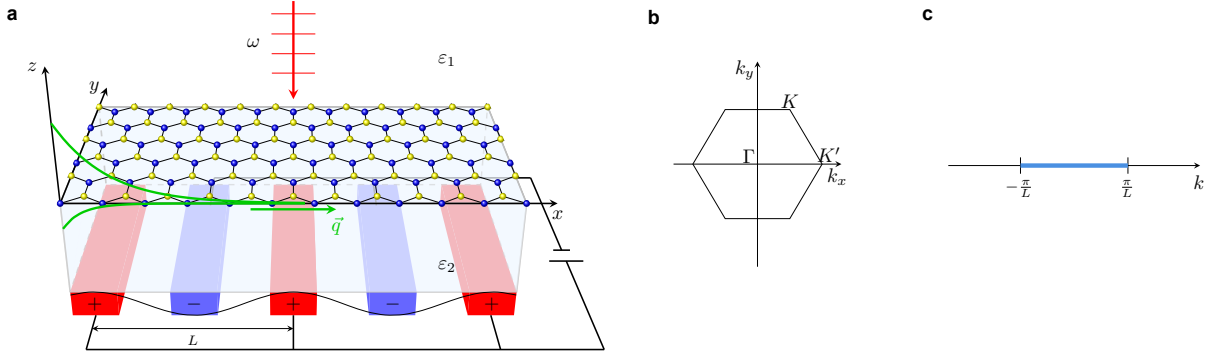


Figure 1: (a) An hBN monolayer over a substrate, subjected to an external periodic potential with period L along the x -direction, under a time-periodic drive of a linearly polarized optical field. The electrostatic gating serves illustrative purposes, as one of the possibilities for achieving the periodic potential. (b) Brillouin zone (BZ) of the original monolayer hBN, and (c) the BZ of the superlattice resulting from applying the 1D potential of (a).

onances used for example in gas sensing.²⁰ At the same time, the interaction of ultraviolet (UV) radiation with the electrons in hBN has promoted the field of UV photonics.²¹

2D materials can be combined by stacking several layers, forming van der Waals heterostructures; materials consisting of few layers have proven to be a fertile theoretical and experimental template for the study of unconventional physics.²² On one hand, heterostructures are promising for tailoring optoelectronic properties of 2D insulators (such as hBN).¹⁸ On the other hand, homostructures reveal quite interesting features, distinct from those of the initial isolated constituents. From the example of AB-stacking graphene bilayer, it was realized that a band gap can be opened and controlled electrostatically, using a voltage bias.^{23,24} In twisted bilayer graphene, it was observed that a superlattice potential has a tremendous impact on the electronic and optical properties of 2D materials.^{25–27} Armed with this information, it is possible to envision a combination of both electrostatic and superlattice potentials such that the electronic and optical properties of 2D materials can be externally controlled. One can manipulate the electronic and optical properties of a material by band-gap engineering.²⁸ For example, it is possible to change the gap of bulk hBN by femtosecond laser pulses.²⁹ For monolayer hBN, the band gap can be reduced by cladding the hBN between two graphene layers,³⁰ or by functionalization.³¹

A previous study on nonlocal quantum plasmonic effects in a graphene one-dimensional (1D) superlattice showed that the external potential can influence the plasmonic properties of graphene.³² Namely, the plasmonic excitations are not affected by the potential along the direction perpendicular to the modulation, but those along the direction of the modulation are drastically modified. In this context, it is pertinent to ask if one can manipulate the physical properties of hBN, the 2D material considered in this work, by forming a superlattice, resulting from combining an hBN lattice with an electrostatic periodic potential (Figure 1a). As a pristine 2D lattice, hBN is a wide-band-gap insulator in which boron (B) and nitrogen (N) atoms are arranged in a honeycomb lattice, bounded by strong covalent bonds. Unlike graphene, hBN presents a large band gap at the K and K'-points of the Brillouin zone (BZ) (see Figure 1b), and the low-energy dispersion is quadratic and not linear, as it is in graphene. In a recent work,³³ a direct measurement of the density of states of monolayer hBN by scanning tunneling microscopy revealed a band gap of 6.8 ± 0.2 eV, while optical spectroscopy revealed an exciton binding energy of 0.7 ± 0.2 eV. With hBN being a large-band-gap insulator, excitonic effects play an important role in its optical properties in the deep UV range.³⁴ This was shown when an experimental measurement of photoluminescence of monolayer hBN on quartz¹⁹ reported an optical resonance around 6.1 eV, that can only be explained by taking excitonic effects into account.

When studying the sub-gap optical properties of hBN, we cannot ignore the fact that the exciton can excite an EM mode confined at the surface of the 2D material, called exciton polariton. The intriguing properties of polaritons allow for the detection of small changes in the refractive index of the surrounding material, rendering the 2D material viable for the fabrication of optoelectronic sensors. Given the energy scales of the band gap and exciton binding energies of hBN, one can think of it as a good candidate for the detection of biomolecules that present resonances in the UV, such as cyclic β -helical peptides, relevant for the biophysics of the human body.³⁵

In this work, we propose a means of manipulating the optoelectronic properties of hBN

by applying a 1D periodic potential on a monolayer, as sketched in Figure 1a. As we will see, the resultant superlattice has distinct electronic properties from the pristine hBN monolayer. The layer is deposited on a quartz substrate of permittivity ε_2 , and is illuminated from above with monochromatic light, linearly polarized along either the x or the y -axis. This driving field allows the formation of excitons that, by coupling with light, give rise to exciton polaritons propagating along the sample. By externally tuning the applied potential, either through its periodicity or its strength (e.g. the gating voltage), the emergence of such polaritons can be engineered over a wide frequency window, from the UV to the infrared, thus providing an efficient means for making the excitonic response of hBN relevant to applications in optics and polaritonics.

2 Results

2.1 Renormalized Hamiltonian

The application of a 1D periodic potential $V(x)$ on top of monolayer hBN results in the low-energy Hamiltonian

$$H = \hbar v_F(\sigma_x q_x + \sigma_y q_y) + M\sigma_z + V(x), \quad (1)$$

where the terms with the Pauli matrices $\sigma_{x/y}$ times momentum $q_{x/y}$ correspond to the low-energy Hamiltonian of hBN, with Fermi velocity v_F given by $\hbar v_F = 5.06 \text{ eV}\cdot\text{\AA}$, and $M = 1.96 \text{ eV}$ being half of the density functional theory (DFT) band gap. These parameters were determined previously by Ferreira et al.³⁴ through first principle calculations, such as DFT and the GW method. To study excitonic physics, it is, in general, sufficient to work with an effective low-energy model, justifying our choice for the starting Hamiltonian of eq 1. The potential $V(x)$ can be realized, for example, by an array of gated metallic rods, very long in length and arranged in parallel, as shown in Figure 1a. With the introduction of the external

potential, we expect to obtain several side-bands as a consequence of the resultant emergent superlattice. Since the Hamiltonian of eq 1 is not written in the most convenient form, as the potential is a function of real-space coordinates, while all other terms are given in momentum space, it is useful to apply a unitary transformation as described in the Methods section. We further assume a potential of the form $V(x) = V_0 \cos(G_0x)$, where V_0 is its amplitude or strength, and $G_0 = 2\pi/L$ is the length of the primitive vector of the reciprocal superlattice and defines the period of the potential, L . Even though Figure 1a depicts the potential with a step-wise form, in what follows we assume a cosine form, as it allows obtaining an analytical expression for the emergent low-energy Hamiltonian; considering a step-wise potential in our calculations would not make a significant difference, as the cosine potential can be seen as the first terms in the Fourier expansion of a step-wise function, and those components are always the strongest ones. Only through analytical calculations, we can obtain the renormalized low-energy Hamiltonian,

$$\bar{H} = \hbar v_F [\sigma_x q_x + \sigma_y J_0(\beta) q_y] - \sigma_z M J_0(\beta), \quad (2)$$

where σ_z is the third Pauli matrix, $J_0(\beta)$ is the Bessel function of the first kind of zeroth order, computed at $\beta = V_0 L / \pi \hbar v_F$, a parameter that only depends on the product between the strength and period of the potential. In eq 2, we notice that for a quasiparticle propagation along the y -direction the group velocity is renormalized as $v_F \rightarrow J_0(\beta) v_F$. Since $|J_0(\beta)| < 1$, the slope of the dispersion along the y -direction is smaller than along the x -direction. This gives rise to an anisotropic Dirac cone. Also, the DFT band gap $E_g = 2M$ changes as $E_g \rightarrow E_g |J_0(\beta)|$. Therefore, it is possible to reduce the pristine gap of hBN by choosing an appropriate value for β . With this mechanism we can control both the gap and the excitonic states, which now become the excitons of a synthetic anisotropic material, that resembles naturally occurring anisotropic materials, such as phosphorene.

From the renormalized low-energy Hamiltonian of eq 2, we can infer the low-energy

dispersion

$$E_s(\mathbf{q}) = \frac{s}{2} \sqrt{E_g^2 J_0^2(\beta) + 4\hbar^2 v_F^2 [q_x^2 + q_y^2 J_0^2(\beta)]}, \quad \text{with } s = +/-, \quad (3)$$

which is now anisotropic, while we recover the isotropic case for $\beta \rightarrow 0$. This deformed paraboloid has two distinct effective masses $m_x = m^* |J_0(\beta)|$ and $m_y = m^* / |J_0(\beta)|$ along the x and y -directions, respectively, where $m^* = E_g / 4v_F^2$ is the electron effective mass in pristine hBN. The eigenproblem $\bar{H}|s, \mathbf{q}\rangle = E_s(\mathbf{q})|s, \mathbf{q}\rangle$ has an analytical solution for the spinors

$$|+, \mathbf{q}\rangle = \begin{pmatrix} e^{-i\theta_q(\beta)} \sin\left(\frac{\xi_q}{2}\right) \\ \cos\left(\frac{\xi_q}{2}\right) \end{pmatrix}, \quad (4a)$$

$$|-, \mathbf{q}\rangle = \begin{pmatrix} \cos\left(\frac{\xi_q}{2}\right) \\ -e^{i\theta_q(\beta)} \sin\left(\frac{\xi_q}{2}\right) \end{pmatrix}, \quad (4b)$$

where $\xi_q = \arctan\left(\frac{2\hbar v_F q(\beta)}{J_0(\beta) E_g}\right)$, with $q(\beta) = \sqrt{q_x^2 + J_0^2(\beta) q_y^2}$, and $\theta_q(\beta) = \arctan[J_0(\beta) \tan \theta]$, with $\tan(\theta) = q_y / q_x$. These spinors will be useful later on to compute the optical conductivity.

It is very relevant to note here that the pristine gap of hBN, the one mentioned in the Introduction, is actually a sum of two contributions: the DFT band gap E_g , and a correction coming from the interaction between electrons.³⁶ The latter, that we will call exchange correction and denote by Δ_{ex} , is computed in Section 2 of the Supporting Information (SI). The true gap of hBN is then $\Delta = E_g + \Delta_{\text{ex}}$, and in the presence of the potential, both contributions renormalize with β .

2.2 Excitonic binding energies

The external 1D potential influences the electronic properties of hBN, as we discussed in the previous section, in a way that depends only on the parameter β , that in turn depends only on the product between the period and strength of the potential, and not on both separately.

Hence, for a complete analysis, it suffices to study the system varying β . As $J_0(\beta) \rightarrow 0$, the dispersion becomes more and more anisotropic, and the DFT gap closes. To study the effects of the potential in the electronic and excitonic properties of the system at hand, we need to compute the *total* band gap Δ , and the binding energies of the excitonic states $1s$, $2x$, $2y$ and $2s$ for varying β , from the case $\beta = 0$ (without potential), to $\beta = 2.3$ (sufficiently close to the first zero of the Bessel function $J_0(\beta)$). To describe the excitonic physics, we adopted the approach of the Wannier equation $E_b\psi = H\psi$, where H is the Hamiltonian for the electron–hole pair, ψ is the exciton wavefunction and E_b its binding energy, and the electrostatic attraction is given by the Rytova–Keldysh potential $V_{\text{RK}}(r) = -\frac{e^2}{4\pi\epsilon_0 r_0} \frac{\pi}{2} \left[\mathbf{H}_0\left(\frac{\kappa r}{r_0}\right) - Y_0\left(\frac{\kappa r}{r_0}\right) \right]$, where κ is the arithmetic average between the static permittivities of the substrate and the surrounding medium, \mathbf{H}_0 is the Struve function of zeroth order, Y_0 is the Bessel function of the second kind and zeroth order, r_0 is a screening parameter of hBN, e is the elementary charge, and ϵ_0 the vacuum permittivity. To solve the Wannier equation, we apply the variational method for the first four excitonic states. For more details, we refer to the Methods section. The results are displayed in Figure 2.

It can be seen in Figure 2a that by manipulating the value of β , we can tune the *total* band gap. When β reaches the zero of $J_0(\beta)$, the gap closes. Regarding the binding energies, Figure 2b shows that the anisotropy lifts the degeneracy between the states $2x$ and $2y$. Also, the binding energies of the states $1s$, $2x$ and $2s$ decrease as we increase β , but that of the $2y$ state is non-monotonic. Nonetheless, the state $2y$ is always the first excited state, as it is always the one with second highest binding energy (in absolute value). Initially, the second excited state is $2x$, but for $\beta \approx 1.5$, the $2s$ takes its place.

2.3 Optical conductivity and Absorption

A recent experimental work¹⁹ showed that single-layer hBN displays optical response in the UV range. The measured photoluminescence exhibits two sharp peaks at a frequency around 6.1 eV. These peaks are excitonic in nature, and their theoretical prediction agrees very well

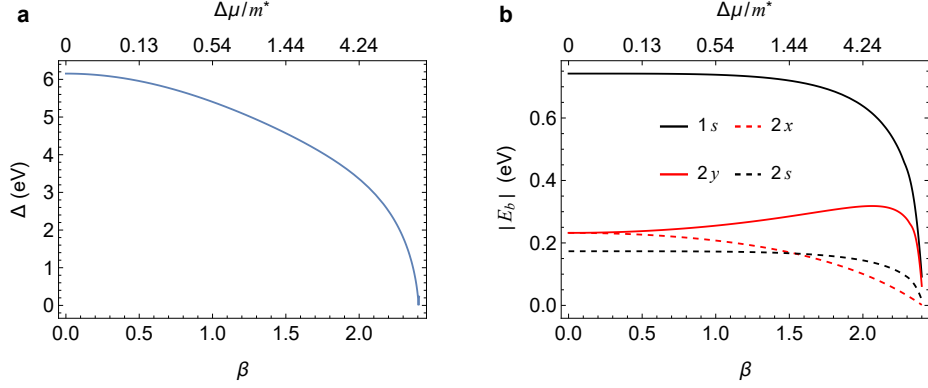


Figure 2: (a) Total band gap of an hBN layer subjected to an 1D periodic potential. (b) Binding energies of the excitonic states $1s$ (black continuous line), $2x$ (red dashed line), $2y$ (red continuous line) and $2s$ (black dashed line) as a function of β . In both panels, the top horizontal axis displays the value of the effective mass anisotropy defined as $\Delta\mu = (m_y - m_x)/m^*$. The parameters used for hBN are:³⁴ $E_g = 3.92$ eV, $\hbar v_F = 5.06$ eV $\cdot\text{\AA}$, and $r_0 = 10$ \AA . For the surrounding medium we assume air with $\varepsilon_1 = 1$, while for the quartz substrate $\varepsilon_2(\omega \rightarrow 0) = 3.9$.

with the experimental measurement³⁶. Here we apply the same theory as Ventura et al.³⁶ to compute the optical absorption of monolayer hBN subjected to the external periodic potential. But first, we computed the optical conductivity using³⁷

$$\sigma(\omega) = \frac{e^2}{8\pi^3 i \hbar} \sum_{\nu} \left[\frac{E_{\nu} |\Omega_{\nu}|^2}{E_{\nu} - (\hbar\omega + i\Gamma)} + \frac{E_{\nu} |\Omega_{\nu}|^2}{E_{\nu} + \hbar\omega + i\Gamma} \right], \quad (5)$$

where E_{ν} is the energy of the excitonic state ν , and Ω_{ν} is a quantity related to the Berry connection, computed from the excitonic wavefunction and the dipole matrix element, whose calculation is explained in the Methods section, with further details in Section S3 of the SI. The conductivity computed through eq 5 for selected values of β , is displayed in Figure 3. Since the optical conductivity is complex, we plot separately the real part in Figure 3a and Figure 3c, and the imaginary part in Figure 3b and Figure 3d. In the calculation we focus on the excitonic states $1s$ and $2s$, while the states $2x$ and $2y$ do not contribute to the conductivity, as explained in Section 3.3 of the SI. We also considered both cases of light polarized along the x and y axes. The results we obtained for the conductivity without potential, corresponding to the blue lines in each panel of Figure 3, agree qualitatively with

those obtained by Ferreira et al. 34 via the Bethe–Salpeter equation method. To be more precise, the behavior of the real part of the conductivity that consists of two peaks centered at the excitonic energy levels in Ferreira et al. 34 is similar to what we compute, and also the imaginary part that changes sign at those levels is identical to what we see in this work. We observe in Figure 3 a tendency of a redshift in the peaks as we increase β , and consequently the anisotropy of the system. We note that the energy level E_ν of the excitonic state ν is given by $E_\nu = E_{b,\nu} + \Delta$, where $E_{b,\nu}$ is the respective binding energy and Δ the *total* band gap, quantities computed previously. For light polarized along the x -axis, we observe in Figure 3a and in Figure 3c that the peaks of the conductivity coming from the $1s$ and $2s$ states are enhanced as we increase β . On the other hand, the peaks in the conductivity for light polarized along the y -direction are attenuated.

One can notice also in Figure 3b that for the case $\beta = 2.3$, the excitonic states $1s$ and $2s$ become so close, that the imaginary part of the conductivity $\Im\{\sigma(\omega)\}$ has only one zero. We expect that this influences the character of the polaritons, since the sign of $\Im\{\sigma(\omega)\}$ dictates which kind of polaritons, transverse magnetic (TM) or transverse electric (TE), the 2D material supports, as we will explain next.

We can now compute the optical absorption at normal incidence using Fresnel’s coefficients and the fact that the absorption, the reflection and the transmission add up to one, as in eq 25. Figure 4a and Figure 4b display the optical absorption for the same values of β as in Figure 3, for light polarized along the x and y -directions, respectively. Interestingly, the behavior of the absorption is not as simple as that of the conductivity. For instance, let us look at Figure 4a. The peak due to the $1s$ state seems to attenuate from right to left, as we increase β . In contrast, the peak due to the $2s$ state seems to intensify. To study this behavior more carefully, in Figure 4c we plot the value of the absorption peaks due to the $1s$ (black lines) and $2s$ (red lines) states separately, for polarization along the x (continuous lines) and y directions (dashed lines), as a function of β , which is allowed to vary continuously. Indeed, we see that for polarization along the x axis the $1s$ peak decreases

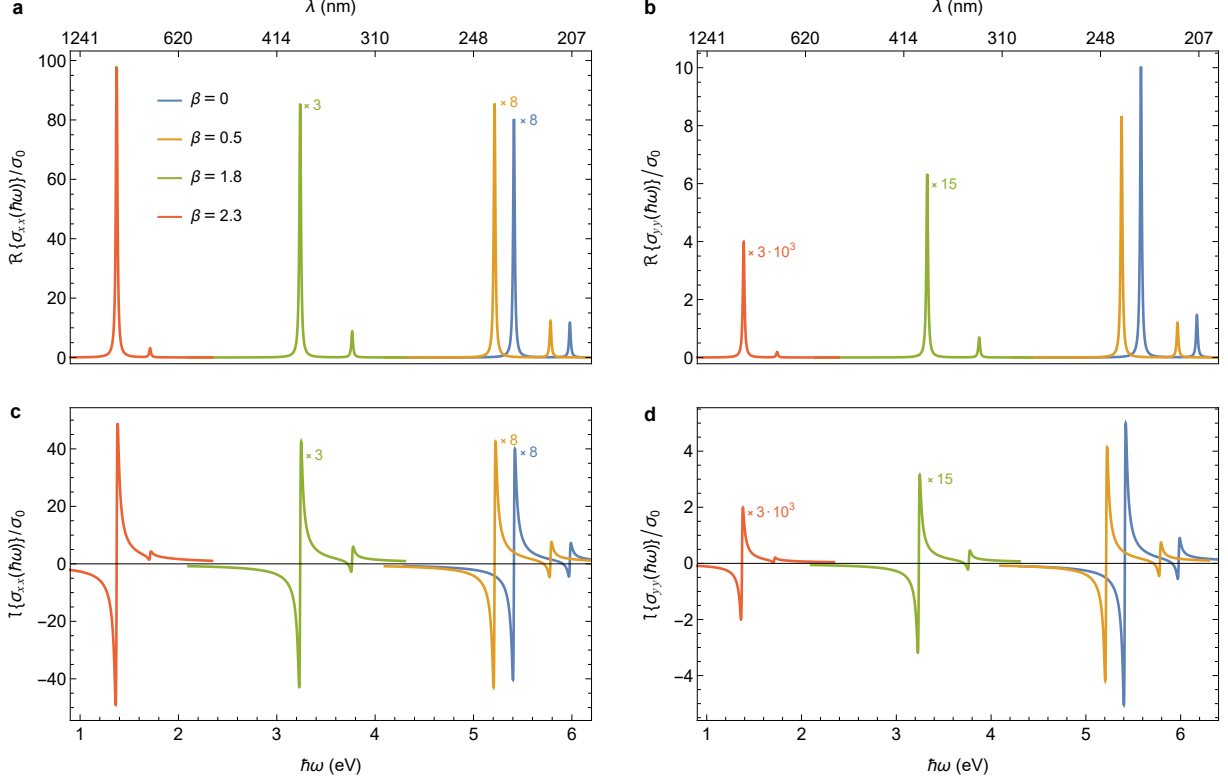


Figure 3: Sub-gap optical conductivity of hBN under a 1D periodic potential, as depicted in Figure 1. Panels (a) and (b) show the real and imaginary parts of the conductivity, respectively, for light polarized along the x -axis. Panels (c) and (d) show the real and imaginary parts of the conductivity, respectively, for light polarized along the y -axis. Results for different β have been rescaled as noted in each panel, for clarity. In eq 5 we use $\Gamma = 10$ meV.

monotonically as we approach the zero of $J_0(\beta)$, while the $2s$ peak tends to increase, until it reaches a maximum right before the zero of the Bessel function. Interestingly, we can have a $2s$ peak more intense than a $1s$ peak. This phenomenon has already been observed experimentally³⁸ and explained theoretically.³⁹ This can be physically clarified by the fact that for high anisotropy in the dispersion and x polarization, the oscillator strength at the $1s$ resonance is very high, thus the material behaves just like a surface of a very high conducting material, such as a metal, reflecting most part of the incident radiation. This can be seen by close inspection of eq 25, which we do at the end of Section S3 in the SI. One can also observe that the absorption for light polarized along the y -direction is not as intense as for light polarized along the x -direction. Furthermore, from Figure 4c, for light polarized along

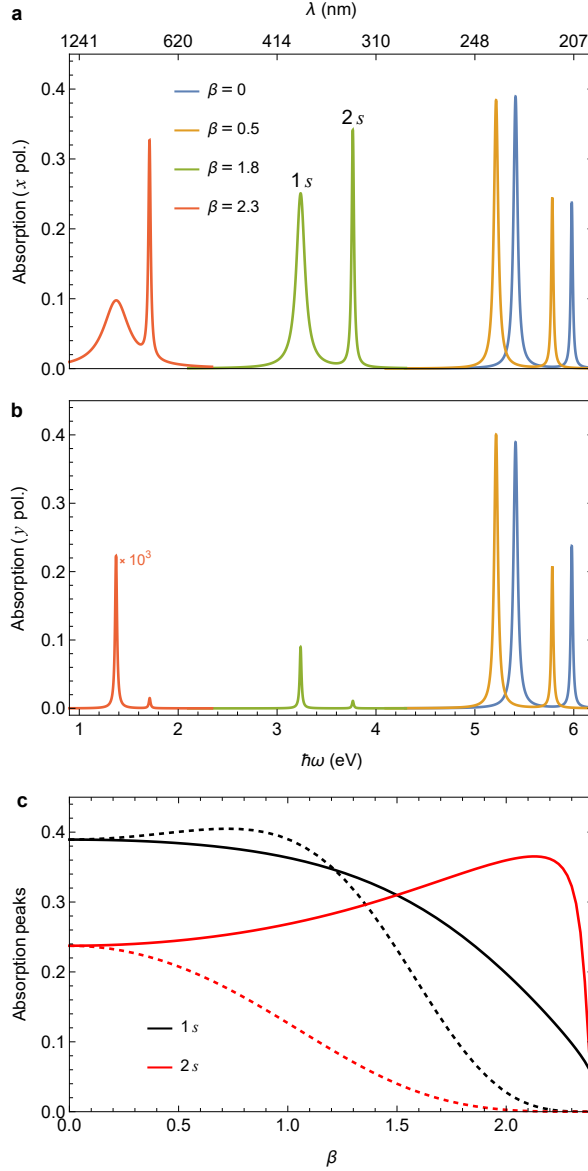


Figure 4: Sub-gap optical absorption of hBN under a 1D periodic potential. Panels (a) and (b) show the absorption for light polarized along the x and y -directions, respectively. Each color corresponds to a different value of β , where $\beta = 0$ corresponds to the case with no potential. We use the same values for β as in Figure 3. For each realization, two peaks are observed. The one occurring at lower energy corresponds to the $1s$ state, while the other corresponds to the $2s$ state. Panel (c) shows the values of the absorption peaks due to the excitonic states $1s$ (black lines) and $2s$ (red lines) as a function of β for light polarized along the x (continuous lines) and y (dashed lines) directions, respectively. Note that for each value of β the peaks occur at different energies, as one can see in panels (a) and (b). For the quartz substrate we use $\varepsilon_2(\omega) \approx 2.16$, an estimated average of the permittivity over a wide range of optical frequencies.

the y -direction we can note that it is now the $2s$ peak that decreases monotonically, while the $1s$ peak is maximum for $\beta \approx 0.9$.

2.4 Exciton polaritons

Polaritons are light-matter hybrids, arising from the strong-coupling of elementary excitations of a 2D material with light. Polaritonic modes are characterized by an evanescent decay away from the material and a strong enhancement of the EM field in its vicinity. There are many kinds of polaritons, like phonon polaritons, plasmon polaritons, magnon polaritons and exciton polaritons.⁴⁰ Here we are concerned only with exciton polaritons. The dispersion relation of the polariton depends on the polarization of the EM field. For TE modes, the electric field is in the plane of the 2D material, and perpendicular to the wavevector of the polariton, while the magnetic field lies on the xz -plane. The dispersion relation for TE modes is

$$\kappa_1 + \kappa_2 - i\omega\mu_0\sigma_{yy}(\omega) = 0, \quad (6)$$

where ε_j , $j = 1, 2$, is the relative electric permittivity of the two media cladding the hBN layer in the frequency region herein considered, $\kappa_j = \sqrt{q^2 - \varepsilon_j\omega^2/c^2}$, ω is the angular frequency of the polariton, q is the in-plane wavenumber, and μ_0 is the vacuum permeability.

For TM modes, it is the magnetic field that lies on the plane of the 2D material, while the electric field is in the xz -plane. Their dispersion relation is

$$\frac{\varepsilon_1}{\kappa_1} + \frac{\varepsilon_2}{\kappa_2} + i\frac{\sigma_{xx}(\omega)}{\varepsilon_0\omega} = 0. \quad (7)$$

As a rule of thumb, TE modes are supported when the imaginary part of the conductivity is negative, whereas TM modes are supported when the imaginary part of the conductivity is positive. The solutions of the previous two equations, that can only be obtained numerically, gives the dispersion relation $\omega(q)$, where the wavenumber has now an imaginary part, since the conductivity is complex. It is important to highlight that in eqs 6 and 7 two different

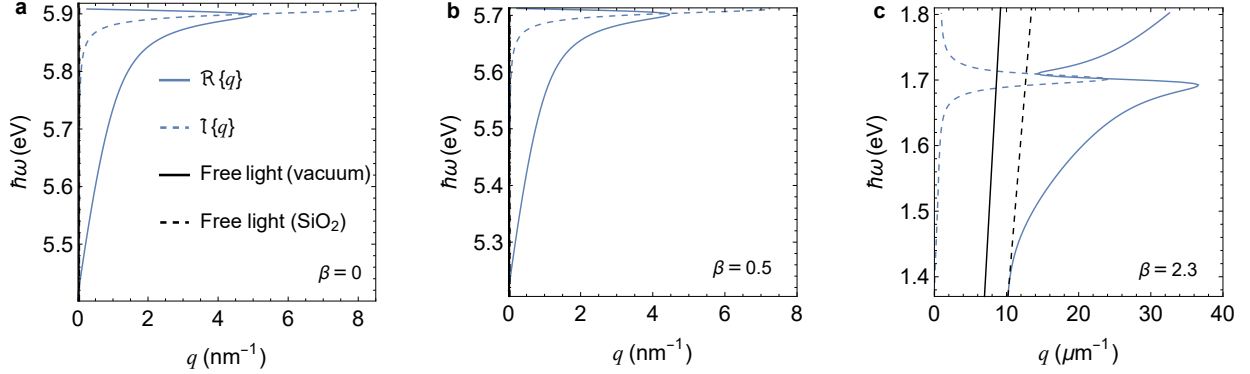


Figure 5: Dispersion relation $\omega(q)$ for TM exciton polaritons, obtained by solving numerically eq 7 for different values of β . The solution is the frequency as a function of the wavenumber, that has a real part (solid blue line) and an imaginary part (dashed blue line). For comparison, we show the dispersion relation for free propagating light in vacuum (solid black line) and in quartz (dashed black line). The case $\beta = 0$ represents monolayer hBN without potential on top. For the quartz substrate, we use $\varepsilon_2(\omega) \approx 2.16$.

conductivities appear. In isotropic systems, such as the case of monolayer hBN, the conductivities σ_{xx} and σ_{yy} coincide. However, they are in general different, as we have seen in the previous section.

Regarding the TE modes, we observe that they are either very poorly confined and present a similar dispersion to free light as expected,^{41,42} or they do not exist at all (that is, eq 6 does not present any solution). Hence, we omit the analysis for TE modes, as they are not relevant. We focus then on TM modes solely. To obtain the dispersion relation $\omega(q)$ for TM polarized polaritons, we solve numerically eq 7 in the regions where $\Im\{\sigma(\omega)\} > 0$, for different values of β . In general, the imaginary part of the conductivity admits more than one zero, and in our case, we have observed in Figure 3 that it has either two or one. The main region of frequencies of interest is that between the first and second zeros, in the case $\Im\{\sigma(\omega)\}$ does have two zeros. After the third zero, we are very near the bottom of the conduction band, where the sub-gap conductivity we computed herein is not accurate. To compute the conductivity above the gap, one needs to also consider unbound states.⁴³

The dispersion relation of TM modes is presented in Figure 5, for three different values of

β . The case $\beta = 0$ (Figure 5a) represents hBN with no potential on top, and we also choose an intermediate case $\beta = 0.5$ (Figure 5b), and an extreme case $\beta = 2.3$ (Figure 5c). The case without potential and the intermediate case share similar features, namely a dispersive behavior very distinct from free light, with the real part of the wavenumber $\Re\{q\}$ reaching a high maximum value at a specific frequency, and the high degree of confinement given the high values that $\Im\{q\}$ can reach. However, the $\beta = 2.3$ case of Figure 5c is qualitatively different. This is due to the fact that in this case the imaginary part of the conductivity has only one zero and the conductivity peaks at higher values. As a consequence, the dispersion behaves like free light in quartz for low frequencies and then behaves like the previous two cases, with $\Re\{q\}$ achieving a maximum around $36 \mu\text{m}^{-1}$. Then, the dispersion bends until $\Re\{q\}$ reaches a minimum of $14 \mu\text{m}^{-1}$, and afterwards it increases back again. This dispersion back-bending is due to the $2s$ resonance, where the oscillator strength increases. The connection between these two effects has been predicted before.⁴⁴ The degree of confinement is also lower in this case, as can be seen by the different wavenumber scales (nm^{-1} in Figure 5a and Figure 5b, μm^{-1} in Figure 5c). To gain intuition on the confinement of the polariton, we show in Figure S2 a spatial map of the EM field of a TM mode in the vicinity of the interface between air and the substrate.

3 Conclusions

With the advent of the experimental realization of 2D materials, the way of manipulating the electronic properties of 2D materials by applying an additional periodic modulation has gained significant attention. Notwithstanding the current popularity of this topic, the idea of forming superlattices to manipulate the properties of materials dates back to the end of the last century, with studies on plasmonic excitations in externally modulated 2D electron-gases.^{45,46} The periodic modulation can result from combining two monolayers to form a bilayer structure and applying a twist to form a moiré superlattice,^{47,48} or even by

combining bulk systems, like for example two hBN slabs, bringing their surfaces together and applying a twist.⁴⁹

In our case, the external potential can be imposed by a periodic patterned back/top gate, as sketched in Figure 1a. The tuning of the potential has a high degree of flexibility, since our predictions depend only on the product of the strength of the potential and its period, but not on both independently. In a typical 3D semiconductor, such as GaAs or CdTe, the exciton size is of the order of 5–12 nm. For the period, we need to choose a high enough value compared to the exciton radius, so of the order of 40 nm. For this length scale, and to have $\beta \sim 1$, we need a potential amplitude of the order of 40 meV, which is feasible in experiments. With these values for the strength of the potential, an hBN flake will not experience atomic reconstruction, as the boron-nitrogen covalent bond in hBN is very strong. However, our theory does not make predictions when β matches exactly the zero of the Bessel function, since the renormalized effective mass along x vanishes and that along y diverges, rendering the Wannier equation description inapplicable. Also, the simplicity of the potential allowed for an analytical expression for the renormalized low-energy Hamiltonian, but it comes with the disadvantage that a cosine potential is more difficult to implement experimentally. We remark that our theory also applies to a square periodic potential, more common in experiments. Hence, our results widely apply to a variety of periodic potentials. Our semi-analytic treatment can also be extended to other 2D semiconductors and substrate materials.

This work presents a way of changing the frequency of the excitonic resonances of hBN, as an alternative to the usual one of changing the substrate. The redshift in the resonances as we increase the strength (or period) of the potential makes it possible to make hBN optically non-trivial in between the near- and the deep-UV. Furthermore, the system response is different depending on the polarization of the incident field, which is the essential characteristic of a grid wire polarizer. Hence, our setup is a possible prototype for the fabrication of very efficient grid polarizers. Beyond that, the characteristics of tunable exciton-polaritons,

namely the ultra-confinement of the EM field and the tuning of the frequency window within which they can be excited, renders our setup also a prototype for the fabrication of sensitive biosensors for organic molecules with different resonant spectra.

The study of excitonic and optical properties in twisted bilayer systems is a natural extension of this work. A key feature in these systems is the emergence of flat electronic bands, enhancing interactions and promoting many-body correlated states, which offer a plethora of exotic phenomena in physics.^{13,15} There are already studies of excitons in these systems^{50,51} that predict that the optical spectrum of the bilayer system is very different from that of the isolated monolayer. Furthermore, plasmon polaritons have been studied in twisted bilayer graphene as well,⁵² where the appearance of electronic flat bands leads to plasmon polaritons with almost constant dispersion. However, polaritonics in the UV range within the realm of twisted bilayer systems remains largely unexplored. With the experimental and technological tools available nowadays, one can expect solid developments in the field of 2D moiré structures in general, and in particular in the study of excitons.^{53,54}

4 Methods

4.1 Renormalized Hamiltonian

The electronic properties of independent electrons in 2D materials can be described, approximately, in terms of tight-binding models; for the tight-binding description to be as realistic as possible, its parameters are determined by first principal methods, such as DFT and *GW*. In general, these models use a fairly large number of bands, which prevents analytical calculations of the materials' properties. Fortunately, the physics of excitons is often determined by effective models with only two bands, whose Hamiltonian can be written using Pauli matrices. These are the cases of graphene and hBN. The difference between the two systems lies in the presence of a band gap in the latter. With all this in mind, an effective, low-energy,

independent-electron Hamiltonian can be written as⁵⁵

$$H_0 = -i\hbar v_F (\sigma_x \partial_x + \sigma_y \partial_y) + M\sigma_z, \quad (8)$$

where $E_g = 2M$ is the band gap obtained within DFT,³⁴ and the σ 's are the Pauli matrices. The low-energy dispersion relation reads

$$E_s(\mathbf{q}) = s \frac{1}{2} \sqrt{E_g^2 + 4\hbar^2 v_F^2 (q_x^2 + q_y^2)} \approx s \left(\frac{E_g}{2} + \frac{\hbar^2 |\mathbf{q}|^2}{2m^*} \right), \quad (9)$$

where the wavevector \mathbf{q} is measured from the \mathbf{K} point in the BZ (see Figure 1b), while $m^* = E_g/2v_F^2$ is the common effective mass of electrons in the conduction band ($s = +1$) and holes in the valence band ($s = -1$), respectively. The approximation of parabolic bands is valid when the DFT band gap is large and when looking at electronic states with small momentum (measured from the point around which we are expanding the Hamiltonian).

Since we want to describe the effect of an external potential on the electronic properties of electrons in hBN (including its excitonic properties), we introduce an external electrostatic potential $V(x)$, so that the total Hamiltonian reads

$$H = H_0 + V(x). \quad (10)$$

The potential varies only along the x -direction and has period L , that is, $V(L+x) = V(x)$. This external potential then creates a superlattice, leading to a mini-BZ of size $[-\pi/L, \pi/L]$, as in Figure 1c, and the appearance of a set of mini-bands. This problem is similar to graphene under an external potential,⁵⁶ but with an extra term that confers a mass to the electrons thus opening an energy gap at K of the original BZ. By introducing the external potential $V(x)$, we add an extra periodicity in the system in addition to the original lattice periodicity (already encoded in the original low-energy Hamiltonian). As noted above, we form a 1D superlattice whose reciprocal lattice vectors are given by $\mathbf{G}_\ell = \ell G_0 \hat{x}$, with

$G_0 = 2\pi/L$ and ℓ an integer.

It would be convenient if we could remove the potential from the Hamiltonian eq 10, while maintaining the Dirac-like form of H_0 . This is possible via a unitary transformation written in terms of $V(x)$ and given by⁵⁶

$$U_\alpha = \frac{1}{\sqrt{2}} \begin{pmatrix} e^{-i\alpha(x)/2} & -e^{i\alpha(x)/2} \\ e^{-i\alpha(x)/2} & e^{i\alpha(x)/2} \end{pmatrix}, \quad (11)$$

where $\alpha(x) = (2/\hbar v_F) \int_0^x dx' V(x')$. Now we rotate the total Hamiltonian in eq 10 to $H \rightarrow H' = U_\alpha^\dagger [H_0 + V(x)] U_\alpha = U_\alpha^\dagger H_0 U_\alpha + V(x)$. The first term is a sum of three contributions, each one going with a Pauli matrix, and it needs to be worked out contribution by contribution. The contribution that goes with σ_z is the simplest, and reads

$$MU_\alpha^\dagger \sigma_z U_\alpha = \begin{pmatrix} 0 & -Me^{i\alpha} \\ -Me^{-i\alpha} & 0 \end{pmatrix}. \quad (12)$$

To work out the contribution that goes with σ_y , we compute the matrix element of that term between two general functions f and g and do an integration by parts in y to write

$$H_y[f, g] = \frac{\hbar v_F}{2} \int d\mathbf{r} f \begin{pmatrix} 0 & -e^{i\alpha(x)} \\ e^{-i\alpha(x)} & 0 \end{pmatrix} \frac{\partial g}{\partial y} - \frac{\hbar v_F}{2} \int d\mathbf{r} \frac{\partial f}{\partial y} \begin{pmatrix} 0 & -e^{i\alpha(x)} \\ e^{-i\alpha(x)} & 0 \end{pmatrix} g \quad (13)$$

To compute the contribution with σ_x , we need to take more care, as the unitary transformation depends on x . In this way, when we rotate that term and integrate by parts, there appear terms where the derivative ∂_x acts only on U_α . When those terms are evaluated, they sum to $-V(x)$, which cancels the potential term in the total Hamiltonian. Then, the terms with σ_x that survive read

$$H_x[f, g] = \frac{-i\hbar v_F}{2} \int d\mathbf{r} f \begin{pmatrix} 0 & e^{i\alpha(x)} \\ e^{-i\alpha(x)} & 0 \end{pmatrix} \frac{\partial g}{\partial x} + \frac{i\hbar v_F}{2} \int d\mathbf{r} \frac{\partial f}{\partial x} \begin{pmatrix} 0 & e^{i\alpha(x)} \\ e^{-i\alpha(x)} & 0 \end{pmatrix} g \quad (14)$$

Focusing on electronic states whose wavevector $\mathbf{k} = \mathbf{q} + \ell \mathbf{G}_0/2$, with $|\mathbf{q}| \ll G_0$, we obtain an analytical expression for the renormalized low-energy Hamiltonian, that is, the initial low-energy Hamiltonian but with renormalized parameters. For that, we use the following states as the basis functions

$$\phi_1 = \begin{pmatrix} 1 \\ 0 \end{pmatrix} e^{i(\mathbf{q} + \ell \mathbf{G}_0/2) \cdot \mathbf{r}} \quad \text{and} \quad \phi_2 = \begin{pmatrix} 0 \\ 1 \end{pmatrix} e^{i(\mathbf{q} - \ell \mathbf{G}_0/2) \cdot \mathbf{r}}, \quad (15)$$

and expand the exponential in a Fourier series as

$$e^{i\alpha(x)} = \sum_{\ell=-\infty}^{\infty} J_\ell(\beta) e^{i\ell G_0 x}, \quad \beta \equiv \frac{V_0 L}{\pi \hbar v_F}, \quad (16)$$

where J_ℓ is the Bessel function of the first kind of order ℓ . The previous identity holds only for a cosine potential. After applying the unitary transformation, we compute the matrix elements for the previous basis states for all the three terms, by replacing f and g with the basis functions. For that, one also has to compute the matrix elements $\langle \phi_i | e^{\pm i\alpha(x)} | \phi_j \rangle = J_0(\beta) \delta_{ij} + J_{\pm\ell}(\beta) \delta_{i1} \delta_{j2} + J_{\mp\ell}(\beta) \delta_{i2} \delta_{j1}$, and replace the spatial derivatives as $\partial_x \rightarrow i(q_x \pm \ell G_0/2)$ and $\partial_y \rightarrow iq_y$. After computing all the matrix elements and summing all the contributions, one obtains for the Hamiltonian

$$\bar{H} = \begin{pmatrix} \hbar v_F (q_x + \ell \frac{G_0}{2}) & i\hbar v_F q_y J_\ell(\beta) - M J_\ell(\beta) \\ -i\hbar v_F q_y J_\ell(\beta) - M J_\ell(\beta) & \hbar v_F (-q_x + \ell \frac{G_0}{2}) \end{pmatrix}, \quad (17)$$

and changing to a basis made of a symmetric and anti-symmetric combination of the previous

states, we obtain the renormalized low-energy Hamiltonian

$$\bar{H}_\ell = \frac{\ell}{2}G_0\hbar v_F + \hbar v_F[\sigma_x q_x + \sigma_y J_\ell(\beta)q_y] - \sigma_z M J_\ell(\beta). \quad (18)$$

Here, the first term simply shifts the energies. Since ℓ is an integer, we have now multiple bands, whose emergence can also be predicted by the theory of nearly-free electrons. The comparison between the two treatments is done in Section 1 of the SI.

To assess the validity of our results, we study eq 18 in the limits $V_0 \rightarrow 0$ and $L \rightarrow \infty$. In both limits, we should obtain the low-energy Hamiltonian of hBN in the absence of the potential. Considering first the limit $V_0 \rightarrow 0$ in eq 18, we obtain

$$\bar{H}_\ell = \frac{\ell}{2}G_0\hbar v_F + \hbar v_F\sigma_x q_x \quad (19)$$

for $\ell \neq 0$, and

$$\bar{H} = \hbar v_F[\sigma_x q_x + \sigma_y q_y] - \sigma_z M \quad (20)$$

for $\ell = 0$. The latter case is simply the original low-energy Hamiltonian of hBN in the absence of potential (with a different sign for the mass term, that does not influence the physics we study here). The former case does not reduce to zero, because it is the Hamiltonian for electronic states with momentum connected to the K point of the original hexagonal BZ by an integer multiple of $G_0\hat{x}/2$, hence the first term is just a global shift in energies that comes from the shift in momentum and the second one is an artifact of measuring momentum along the x direction around the edges of mini Brillouin zones of the superlattice that no longer exists

Considering now the case of $L \rightarrow \infty$, we should also recover the original low-energy Hamiltonian, as this case corresponds to a potential with infinite period, i.e., a constant potential. Looking again at eq 18, we note that for each ℓ we have a different Hamiltonian.

Writing the total Hamiltonian including all the bands as

$$\begin{aligned}
H_{\text{total}} &= \sum_{\ell} \bar{H}_{\ell} = \\
&= \sum_{\ell} \frac{\ell}{2} G_0 \hbar v_F + \hbar v_F [\sigma_x q_x + \sigma_y q_y \sum_{\ell} J_{\ell}(\beta)] - \sigma_z M \sum_{\ell} J_{\ell}(\beta) = \\
&\stackrel{L \rightarrow \infty}{=} \hbar v_F [\sigma_x q_x + \sigma_y q_y] - \sigma_z M,
\end{aligned} \tag{21}$$

where in the last equality we took the limit $L \rightarrow \infty$, and used the fact that $G_0 \propto 1/L \rightarrow 0$ and the property $\sum_{\ell} J_{\ell}(\beta) = 1$ of the Bessel functions of the first kind. In this way, we recovered the original low-energy Hamiltonian of hBN (again with the mass term sign flipped).

4.2 Excitonic contributions to sub-gap optical response

The presence of the external potential $V(x)$ influences considerably the electronic properties of hBN, by rendering the low-energy dispersion anisotropic. This brings consequences to the excitonic physics, and subsequently to the optical response. There are several approaches to the calculation of the excitonic properties of a semiconductor or a band insulator. Excitons with a radius large enough compared to the lattice spacing are denoted Wannier excitons. The general approach to determine the exciton energy levels and wavefunctions is the solution of the Bethe–Salpeter equation⁵⁷ in momentum space. This microscopic approach is powerful but often computationally demanding. It would then be desirable to have in reach a simpler approach that still captures the essence of the exciton physics. Starting from a microscopic approach,⁵⁸ if the dispersion is quadratic in momentum and the DFT band gap is large, then the Fourier transform of the Bethe–Salpeter equation transforms into an effective Schrödinger equation with an electrostatic attractive potential called the Wannier equation (see further details in Section 2 of the SI). The method of the Wannier equation has been benchmarked against the Bethe–Salpeter equation with good results, as the latter equation accounts for fine details only.⁵⁸

The Wannier equation can be solved, among others, with the variational method, which allows for a good approximation of the energies and approximate analytical expressions for the excitonic wavefunctions. This approach has previously been applied to black phosphorus⁵⁹ and TMDs,^{60,61} with significant accuracy.

4.2.1 Variational method

The variational method⁶² consists in using a trial wavefunction, that depends on a set of parameters, to compute the expectation value of the Hamiltonian H and minimize it with respect to said parameters. Symbolically, we define a state $|\psi_\alpha(\mathbf{r})\rangle$, with α representing the set of unknown parameters. Then we compute $E_\alpha = \langle \psi_\alpha(\mathbf{r}) | H | \psi_\alpha(\mathbf{r}) \rangle$ and solve $\partial E / \partial \alpha = 0$ for α . Finally, we return to E_α and substitute the optimal values for α .

The Hamiltonian H pertains to the system comprised of an electron–hole pair,

$$H = \frac{p_x^2}{2\mu_x} + \frac{p_y^2}{2\mu_y} + V_{\text{RK}}(r), \quad (22)$$

where the first two terms correspond to the kinetic contribution, with μ_x and μ_y being the electron–hole reduced masses along the x and y -directions, respectively, and the last term corresponding to the electrostatic attraction between the electron and the hole in the 2D material, here given by the electrostatic Rytova–Keldysh potential⁵⁷

$$V_{\text{RK}}(r) = -\frac{e^2}{4\pi\epsilon_0 r_0} \frac{\pi}{2} \left[\mathbf{H}_0 \left(\frac{\kappa r}{r_0} \right) - Y_0 \left(\frac{\kappa r}{r_0} \right) \right]. \quad (23)$$

In our work, the surrounding medium is air ($\epsilon_1 = 1$), while for the substrate we choose silicon dioxide (SiO_2). The static dielectric function of quartz is $\epsilon_2(\omega \rightarrow 0) = 3.9$, and in the UV range it is essentially constant, with $\epsilon_2(\omega) \approx 2.16$. As mentioned previously in the "Excitonic binding energies" section, the exciton dynamics is determined by the Wannier equation $E_b \psi = H \psi$, which is a Schrödinger-like equation, where H is the Hamiltonian given in eq 22, ψ is the exciton wavefunction and $E_b = E - \Delta$ is the exciton binding energy,

while E is the energy level of the exciton and Δ the total band gap. To obtain the energy levels of the exciton we have to compute the binding energies and Δ . For the former, we apply the variational method to the first four excitonic states $1s$, $2x$, $2y$ and $2s$, and use trial wavefunctions that resemble the solutions of the 2D hydrogen atom, but taking into account the effect of the anisotropy in the mass tensor. The form of each wavefunction is given in Section 3.1 of the SI, eqs S.10a-d, and the details of the calculations for finding the variational parameters are given in Mikhail et al.⁵⁹ The total band gap is the sum of the renormalized DFT gap and the electron–electron exchange correction, both contributions renormalizing with the potential (see Section 2 of the SI for details).

4.2.2 Optical conductivity

Subjecting the excitonic material to an external and monochromatic EM field with frequency ω , the optical conductivity, within linear response and in the dipole approximation, is given by eq 5, and it can be obtained within perturbation theory. However, the derivation is lengthy and not straightforward, so for further details we refer to Pedersen et al.³⁷ The broadening parameter $\Gamma \ll \omega$ is the sum of the non-radiative decay due to phonons, the non-radiative decay due to impurities and the radiate decay, but its calculation is outside the scope of this work. Therefore, we made an estimation based on previous works.³⁶ Furthermore, Ω_ν is related to the Berry curvature $\mathbf{\Omega}_{cv,\mathbf{q}} = iV_{\text{UC}}^{-1} \int_{\text{UC}} u_{+,\mathbf{q}}^* \nabla_{\mathbf{q}} u_{-,\mathbf{q}} d\mathbf{r}$, with V_{UC} being the volume of the unit cell and $u_{\pm,\mathbf{q}}$ the Bloch wavefunctions of the conduction and valence bands, for + and –, respectively, and the excitonic state ν through

$$\Omega_\nu = \sum_{\mathbf{q}} \Psi_\nu(\mathbf{q}) \hat{\mathbf{e}} \cdot \mathbf{\Omega}_{cv,\mathbf{q}}, \quad (24)$$

where $\Psi_\nu(\mathbf{q})$ is the wavefunction of the excitonic state ν in momentum space, and the unit vector $\hat{\mathbf{e}}$ is dictated by the polarization of the wave. We can identify the Berry curvature $\mathbf{\Omega}_{cv,\mathbf{q}}$ with the dipole matrix element between those bands. One simply considers i times

the gradient operator in momentum space as the position operator \mathbf{r} . In this way, $\Omega_{cv,\mathbf{q}} = \langle +, \mathbf{q} | \mathbf{r} | -, \mathbf{q} \rangle$, where the bra/ket corresponds to the spinor of the Hamiltonian (eq 2) for the conduction/valence band. Herein we consider light polarized along either the x and the y -directions. As the system is anisotropic, the conductivity will be different depending on the polarization of the incident EM field. As explained in Section 3 of the SI, we have two distinct conductivities σ_{xx} and σ_{yy} for light polarized along the x and y -directions, respectively. Knowing the optical conductivity, we compute the sub-gap optical absorption through

$$\mathcal{A} = 1 - \mathcal{R} - \Re \left\{ \sqrt{\frac{\varepsilon_2}{\varepsilon_1}} \right\} \mathcal{T}, \quad (25)$$

where the reflection and transmission coefficients \mathcal{R} and \mathcal{T} follow from Fresnel's equations for normal incidence on a conductive material cladded between two dielectrics.⁴¹ We note that the relative permittivities that enter in eq 25 are the dynamic dielectric functions of the respective materials. In the electron–electron or electron–hole interaction, the relevant quantities are the static permittivities of the materials. In the end, the dependence is only on the average between the static permittivities, that we denoted by κ in eq 23.

Acknowledgement

N. A. M. is a VILLUM Investigator supported by VILLUM FONDEN (Grant No. 16498). The Center for Polariton-driven Light–Matter Interactions (POLIMA) is funded by the Danish National Research Foundation (Project No. DNRF165). This project was supported by the Independent Research Fund Denmark (grant no. 2032-00045A). N. M. R. P. acknowledges support by the Portuguese Foundation for Science and Technology (FCT) in the framework of the Strategic Funding UIDB/04650/2020, COMPETE 2020, PORTUGAL 2020, FEDER, and through projects PTDC/FIS-MAC/2045/2021 and EXPL/FIS-MAC/0953/2021. N. M. R. P. also acknowledges the Independent Research Fund Denmark (grant no. 2032-00045B) and the Danish National Research Foundation (Project

No. DNR165).

Supporting Information Available

Conciliating nearly-free electron theory with the analytical method, calculation of the electron–electron exchange correction to the electronic band gap, calculation of the optical conductivity, and spatial map of the electromagnetic field of the polariton.

References

- (1) Jiang, H.; Zheng, L.; Liu, Z.; Wang, X. Two-Dimensional Materials: From Mechanical Properties to Flexible Mechanical Sensors. *InfoMat* **2020**, *2*, 1077–1094.
- (2) Dutta, T.; Yadav, N.; Wu, Y.; Cheng, G. J.; Liang, X.; Ramakrishna, S.; Sbai, A.; Gupta, R.; Mondal, A.; Hongyu, Z.; Yadav, A. Electronic Properties of 2D Materials and their Junctions. *Nano Mater. Sci.* **2023**, DOI: 10.1016/j.nanoms.2023.05.003.
- (3) Jia, B. 2D Optical Materials and the Implications for Photonics. *APL Photonics* **2019**, *4*, 080401.
- (4) Gan, X.; Mak, K. F.; Gao, Y.; You, Y.; Hatami, F.; Hone, J.; Heinz, T. F.; Englund, D. Strong Enhancement of Light–Matter Interaction in Graphene Coupled to a Photonic Crystal Nanocavity. *Nano Lett.* **2012**, *12*, 5626–5631.
- (5) Geim, A. K.; Novoselov, K. S. The Rise of Graphene. *Nat. Mater.* **2007**, *6*, 183–191.
- (6) Miller, J. L. A Family of Two-Dimensional Conductors Comes into Bloom. *Phys. Today* **2023**, *76*(6), 12.
- (7) Song, X.; Hu, J.; Zeng, H. Two-Dimensional Semiconductors: Recent Progress and Future Perspectives. *J. Mater. Chem. C* **2013**, *1*, 2952–2969.

- (8) Huang, X.; Liu, C.; Zhou, P. 2D Semiconductors for Specific Electronic Applications: from Device to System. *npj 2D Mater. Appl.* **2022**, *6*, 51.
- (9) Cao, Y.; Chowdhury, D.; Rodan-Legrain, D.; Rubies-Bigorda, O.; Watanabe, K.; Taniguchi, T.; Senthil, T.; Jarillo-Herrero, P. Strange Metal in Magic-Angle Graphene with Near Planckian Dissipation. *Phys. Rev. Lett.* **2020**, *124*, 076801.
- (10) Jiang, Z.; Wang, P.; Jiang, X.; Zhao, J. MBene (MnB): a New Type of 2D Metallic Ferromagnet with High Curie Temperature. *Nanoscale Horiz.* **2018**, *3*, 335–341.
- (11) Yu, S.; Li, X.; Tang, J.; Wang, Y.; Xu, F.; Wang, X. Recent Advances in Two-Dimensional Ferromagnetism: Strain-, Doping-, Structural- and Electric Field-Engineering toward Spintronic Applications. *Sci. Technol. Adv. Mater.* **2022**, *23*, 140–160.
- (12) Qiu, D.; Gong, C.; Wang, S.; Zhang, M.; Yang, C.; Wang, X.; Xiong, J. Recent Advances in 2D Superconductors. *Adv. Mater.* **2021**, *33*, 2006124.
- (13) Cao, Y.; Fatemi, V.; Fang, S.; Watanabe, K.; Taniguchi, T.; Kaxiras, E.; Jarillo-Herrero, P. Unconventional Superconductivity in Magic-Angle Graphene Superlattices. *Nature* **2018**, *556*, 43–50.
- (14) Park, J. M.; Cao, Y.; Watanabe, K.; Taniguchi, T.; Jarillo-Herrero, P. Tunable Strongly Coupled Superconductivity in Magic-Angle Twisted Trilayer Graphene. *Nature* **2021**, *590*, 249–255.
- (15) Cao, Y.; Fatemi, V.; Demir, A.; Fang, S.; Tomarken, S. L.; Luo, J. Y.; Sanchez-Yamagishi, J. D.; Watanabe, K.; Taniguchi, T.; Kaxiras, E.; Ashoori, R. C.; Jarillo-Herrero, P. Correlated Insulator Behaviour at Half-Filling in Magic-Angle Graphene Superlattices. *Nature* **2018**, *556*, 80–84.

- (16) Abidi, I. H.; Mendelson, N.; Tran, T. T.; Tyagi, A.; Zhuang, M.; Weng, L.-T.; Özyilmaz, B.; Aharonovich, I.; Toth, M.; Luo, Z. Selective Defect Formation in Hexagonal Boron Nitride. *Adv. Opt. Mater.* **2019**, *7*, 1900397.
- (17) Banszerus, L.; Schmitz, M.; Engels, S.; Goldsche, M.; Watanabe, K.; Taniguchi, T.; Beschoten, B.; Stampfer, C. Ballistic Transport Exceeding 28 μm in CVD Grown Graphene. *Nano Lett.* **2016**, *16*, 1387–1391.
- (18) Rizzo, D. J. et al. Polaritonic Probe of an Emergent 2D Dipole Interface. *Nano Lett.* **2023**, *23*, 8426–8435.
- (19) Elias, C.; Valvin, P.; Pelini, T.; Summerfield, A.; Mellor, C. J.; Cheng, T. S.; Eaves, L.; Foxon, C. T.; Beton, P. H.; Novikov, S. V.; Gil, B.; Cassabois, G. Direct Band-Gap Crossover in Epitaxial Monolayer Boron Nitride. *Nat. Commun.* **2019**, *10*, 2639.
- (20) Yang, W.; Ang, L. K.; Zhang, W.; Han, J.; Xu, Y. High Sensitivity Gas Sensor Based on Surface Exciton Polariton Enhanced Photonic Spin Hall Effect. *Opt. Express* **2023**, *31*, 27041–27053.
- (21) Li, S.; Pershin, A.; Thiering, G.; Udvarhelyi, P.; Gali, A. Ultraviolet Quantum Emitters in Hexagonal Boron Nitride from Carbon Clusters. *J. Phys. Chem. Lett.* **2022**, *13*, 3150–3157.
- (22) Geim, A. K.; Grigorieva, I. V. Van der Waals Heterostructures. *Nature* **2013**, *499*, 419–425.
- (23) Henriques, J. C. G.; Amorim, B.; Ribeiro, R. M.; Peres, N. M. R. Excitonic Response of AA' and AB Stacked hBN Bilayers. *Phys. Rev. B* **2022**, *105*, 115421.
- (24) Castro, E. V.; Novoselov, K. S.; Morozov, S. V.; Peres, N. M. R.; dos Santos, J. M. B. L.; Nilsson, J.; Guinea, F.; Geim, A. K.; Neto, A. H. C. Biased Bilayer Graphene:

- Semiconductor with a Gap Tunable by the Electric Field Effect. *Phys. Rev. Lett.* **2007**, *99*, 216802.
- (25) Bistritzer, R.; MacDonald, A. H. Moiré Bands in Twisted Double-Layer Graphene. *Proc. Nat. Acad. Sci. U. S. A.* **2011**, *108*, 12233–12237.
- (26) Lopes dos Santos, J. M. B.; Peres, N. M. R.; Castro Neto, A. H. Graphene Bilayer with a Twist: Electronic Structure. *Phys. Rev. Lett.* **2007**, *99*, 256802.
- (27) Hennighausen, Z.; Kar, S. Twistronics: a Turning Point in 2D Quantum Materials. *Electron. Struct.* **2021**, *3*, 014004.
- (28) Chaves, A. et al. Bandgap Engineering of Two-Dimensional Semiconductor Materials. *npj 2D Mater. Appl.* **2020**, *4*, 29.
- (29) Xue, L. et al. Unraveling Ultrafast Photoionization in Hexagonal Boron Nitride. 2021, 2101.10429v2, arXiv (Optics). <https://arxiv.org/abs/2101.10429> (accessed 12-04-2023).
- (30) Thygesen, K. S. Calculating Excitons, Plasmons, and Quasiparticles in 2D Materials and van der Waals Heterostructures. *2D Materials* **2017**, *4*, 022004.
- (31) Bhattacharya, A.; Bhattacharya, S.; Das, G. P. Band Gap Engineering by Functionalization of BN Sheet. *Phys. Rev. B* **2012**, *85*, 035415.
- (32) Brey, L.; Stauber, T.; Martín-Moreno, L.; Gómez-Santos, G. Nonlocal Quantum Effects in Plasmons of Graphene Superlattices. *Physical Review Letters* **2020**, *124*, 257401.
- (33) Román, R. J. P.; Costa, F. J. R. C.; Zobelli, A.; Elias, C.; Valvin, P.; Cassabois, G.; Gil, B.; Summerfield, A.; Cheng, T. S.; Mellor, C. J.; Beton, P. H.; Novikov, S. V.; Zagonel, L. F. Band Gap Measurements of Monolayer h-BN and Insights into Carbon-Related Point Defects. *2D Materials* **2021**, *8*, 044001.

- (34) Ferreira, F.; Chaves, A. J.; Peres, N. M. R.; Ribeiro, R. M. Excitons in Hexagonal Boron Nitride Single-Layer: a New Platform for Polaritonics in the Ultraviolet. *J. Opt. Soc. Am. B* **2019**, *36*, 674–683.
- (35) Fears, K. P.; Petrovykh, D. Y.; Photiadis, S. J.; Clark, T. D. Circular Dichroism Analysis of Cyclic β -Helical Peptides Adsorbed on Planar Fused Quartz. *Langmuir* **2013**, *29*, 10095–10101.
- (36) Henriques, J. C. G.; Ventura, G. B.; Fernandes, C. D. M.; Peres, N. M. R. Optical Absorption of Single-Layer Hexagonal Boron Nitride in the Ultraviolet. *J. Phys.: Cond. Matter* **2019**, *32*, 025304.
- (37) Pedersen, T. G. Intraband Effects in Excitonic Second-Harmonic Generation. *Phys. Rev. B* **2015**, *92*, 235432.
- (38) Ju, L.; Wang, L.; Cao, T.; Taniguchi, T.; Watanabe, K.; Louie, S. G.; Rana, F.; Park, J.; Hone, J.; Wang, F.; McEuen, P. L. Tunable Excitons in Bilayer Graphene. *Science* **2017**, *358*, 907–910.
- (39) Henriques, J. C. G.; Epstein, I.; Peres, N. M. R. Absorption and Optical Selection Rules of Tunable Excitons in Biased Bilayer Graphene. *Phys. Rev. B* **2022**, *105*, 045411.
- (40) Basov, D. N.; Asenjo-Garcia, A.; Schuck, P. J.; Zhu, X.; Rubio, A. Polariton Panorama. *NanoPhotonics* **2021**, *10*, 549–577.
- (41) Bludov, Y. V.; Ferreira, A.; Peres, N. M. R.; Vasilevskiy, M. I. A PRIMER ON SURFACE PLASMON-POLARITONS IN GRAPHENE. *Int. J. Mod. Phys. B* **2013**, *27*, 1341001.
- (42) Gonçalves, P. A. D.; Peres, N. M. R. *An Introduction to Graphene Plasmonics*; World Scientific: SinGapore, 2016.

- (43) Leppenen, N. V.; Golub, L. E.; Ivchenko, E. L. Sommerfeld Enhancement Factor in Two-Dimensional Dirac Materials. *Phys. Rev. B* **2021**, *103*, 235311.
- (44) Wolff, C.; Busch, K.; Mortensen, N. A. Modal Expansions in Periodic Photonic Systems with Material Loss and Dispersion. *Phys. Rev. B* **2018**, *97*, 104203.
- (45) van Zyl, B. P.; Zaremba, E. Thomas–Fermi–Dirac–von Weizsäcker Hydrodynamics in Laterally Modulated Electronic Systems. *Phys. Rev. B* **1999**, *59*, 2079–2094.
- (46) Fessatidis, V.; Cui, H. L. Hydrodynamic Theory of Magnetoplasmons in a Modulated Two-Dimensional Electron Gas. *Phys. Rev. B* **1991**, *43*, 11725–11731.
- (47) Chu, Y.; Liu, L.; Yuan, Y.; Shen, C.; Yang, R.; Shi, D.; Yang, W.; Zhang, G. A Review of Experimental Advances in Twisted Graphene Moiré Superlattice. *Chin. Physics B* **2020**, *29*, 128104.
- (48) Yan, W.; Meng, L.; Meng, Z.; Weng, Y.; Kang, L.; Li, X.-a. Probing Angle-Dependent Interlayer Coupling in Twisted Bilayer WS₂. *J. Phys. Chem. C* **2019**, *123*, 30684–30688.
- (49) Lee, H. Y.; Al Ezzi, M. M.; Raghuvanshi, N.; Chung, J. Y.; Watanabe, K.; Taniguchi, T.; Garaj, S.; Adam, S.; Gradečak, S. Tunable Optical Properties of Thin Films Controlled by the Interface Twist Angle. *Nano Lett.* **2021**, *21*, 2832–2839.
- (50) Brem, S.; Malic, E. Bosonic Delocalization of Dipolar Moiré Excitons. *Nano Lett.* **2023**, *23*, 4627–4633.
- (51) Roman-Taboada, P.; Obregon-Castillo, E.; Botello-Mendez, A. R.; Noguez, C. Excitons in Twisted AA′ Hexagonal Boron Nitride Bilayers. *Phys. Rev. B* **2023**, *108*, 075109.
- (52) Stauber, T.; Kohler, H. Quasi-Flat Plasmonic Bands in Twisted Bilayer Graphene. *Nano Lett.* **2016**, *16*, 6844–6849.

- (53) Wu, B.; Zheng, H.; Li, S.; Ding, J.; He, J.; Zeng, Y.; Chen, K.; Liu, Z.; Chen, S.; Pan, A.; Liu, Y. Evidence for Moiré Intralayer Excitons in Twisted WSe₂/WSe₂ Homobilayer Superlattices. *Light Sci. Appl.* **2022**, *11*, 166.
- (54) Zhao, S.; Li, Z.; Huang, X.; Rupp, A.; Göser, J.; Vovk, I. A.; Kruchinin, S. Y.; Watanabe, K.; Taniguchi, T.; Bilgin, I.; Baimuratov, A. S.; Högele, A. Excitons in Mesoscopically Reconstructed Moiré Heterostructures. *Nat. Nanotechnol.* **2023**, *18*, 572–579.
- (55) Castro Neto, A. H.; Guinea, F.; Peres, N. M. R.; Novoselov, K. S.; Geim, A. K. The Electronic Properties of Graphene. *Rev. Mod. Phys.* **2009**, *81*, 109–162.
- (56) Park, C.-H.; Yang, L.; Son, Y.-W.; Cohen, M. L.; Louie, S. G. New Generation of Massless Dirac Fermions in Graphene under External Periodic Potentials. *Phys. Rev. Lett.* **2008**, *101*, 126804.
- (57) Quintela, M. F. C. M.; Henriques, J. C. G.; Tenório, L. G. M.; Peres, N. M. R. Theoretical Methods for Excitonic Physics in 2D Materials. *phys. stat. solid. (b)* **2022**, *259*, 2200097.
- (58) Have, J.; Catarina, G.; Pedersen, T. G.; Peres, N. M. R. Monolayer Transition Metal Dichalcogenides in Strong Magnetic Fields: Validating the Wannier Model Using a Microscopic Calculation. *Phys. Rev. B* **2019**, *99*, 035416.
- (59) Gomes, J. N. S.; Trallero-Giner, C.; Vasilevskiy, M. I. Variational Calculation of the Lowest Exciton States in Phosphorene and Transition Metal Dichalcogenides. *J. Phys.: Cond. Matter* **2021**, *34*, 045702.
- (60) Martins Quintela, M. F. C.; Peres, N. M. R. A Colloquium on the Variational Method Applied to Excitons in 2D Materials. *Eur. Phys. J. B* **2020**, *93*, 222.
- (61) Henriques, J. C. G.; Mortensen, N. A.; Peres, N. M. R. Analytical Description of the

1s Exciton Linewidth Temperature Dependence in Transition Metal Dichalcogenides.
Phys. Rev. B **2021**, *103*, 235402.

(62) Sakurai, J. J.; Napolitano, J. *Modern Quantum Mechanics*, 3rd ed.; Cambridge University Press, 2020.

TOC Graphic

